LANGMUIR Article
Cite This: Langmuir 2018, 34, 12379−12386
pubs.acs.org/Langmuir

Arrested Coalescence of Viscoelastic Droplets: Ellipsoid Shape Effects and Reorientation

Chen Hao,[†] Zhaoyu Xie,[‡] Timothy J. Atherton,[‡] and Patrick T. Spicer*[,†]

[†]School of Chemical Engineering, UNSW Sydney, Sydney, New South Wales 2052, Australia
[‡]Department of Physics and Astronomy, Tufts University, Boston, Massachusetts 02155, United States

Supporting Information

ABSTRACT: The stable configurations formed by two poroelastic, ellipsoid-shaped droplets during their arrested coalescence have been investigated using micromanipulation experiments. Ellipsoidal droplets are produced by millifluidic emulsification of petrolatum into a yield stress fluid that preserves their elongated shape. The liquid meniscus between droplets can transmit stress and instigate movement of the droplets, from their initial relative position, in order to minimize doublet surface energy. The action of the liquid meniscus causes the ellipsoidal droplets to undergo rolling and reorientation events because of their unique ellipsoid shape and associated variation in the surface curvature. The final configuration of the droplets is controlled by the balance between interfacial Laplace pressure and internal elasticity, as well as a constraint force that resists complete minimization of surface energy. Geometric and surface energy calculations are used to map the possible and most likely configurations of the droplet pairs. Experimental deviations from the calculations indicate the magnitude and potential origin of the constraint force resisting full equilibration. Droplet aspect ratio and elasticity are both shown to influence the degree of reorientation and stability of the droplets at energy extrema. Higher aspect ratios drive greater reorientation and better agreement with final doublet configurations predicted by energy minimization. Lower elasticity droplets undergo secondary deformations at high aspect ratios, further broadening the space of possible morphologies.

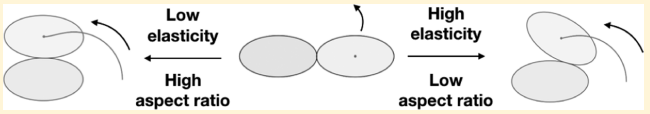

INTRODUCTION

Emulsions are broadly used in food,[1] pharmaceutical,[2] polymeric,[3] petroleum,[4] biomimetic,[5,6] bijel,[7] and even explosive[8] materials. Coalescence, when emulsion droplets combine into a larger fluid volume, is a critical dynamic in commercial products. Coalescence can be harmful, when product instabilities occur, or beneficial, when it imparts rheology modification and desirable texture to a fluid like whipped cream.

Arrested coalescence occurs when coalescence begins minimizing the droplet surface energy but is halted by a physical resistance such as interfacial or internal droplet elasticity.[9−11] Arrested coalescence is commonly observed in dairy products, where a network of solid milk fat crystals forms inside of oil droplets.[12] The poroelasticity of the droplet allows coalescence to begin because of the liquid phase permeating the solid crystal skeleton but is then halted when the crystal structure cannot be deformed enough for full coalescence.[10,11] Arrested coalescence is important to the study of food products, as it is a key phenomenon used to build structure, texture, and aesthetic perception of most dairy products,[13] but recent work has shown applications of arrested droplets in other materials as well.

Colloidal materials are often developed under conditions when arrested coalescence is significant, as when partially molten metal particles assemble into clusters[14] or when evaporating films of solvent squeeze suspended particles or droplets.[15−18] The final structure and performance of such systems are highly dependent on the packing and structure of constituent spherical colloids, and it is important to know the effects of dynamic capillary processes in these systems on the evolution of structure as assembly proceeds. For example, it was shown recently that spherical viscoelastic droplets can significantly reorient as a result of liquid capillary effects during arrested coalescence, spontaneously driving the droplets into more compact packing arrangements even though initially added at less-optimal positions.[19] However, meniscus effects also play a significant role in shape changes by aggregates of nonspherical solid colloids, enhancing self-assembly,[20−23] sintering of metal structures,[18] additive manufacturing,[24] and aggregation of nonspherical fat solids.[25]

Droplets are typically spherical because interfacial tension acts to minimize surface energy. In some viscoelastic droplets, however, the internal rheology of the droplets can preserve nonspherical shapes[26−28] and is used to enhance deposition onto biological surfaces[29,30] and food emulsion rheology.[31−33] There is then also a need to understand arrested coalescence and its shape-change dynamics for nonspherical droplets. We are interested in these dynamics for two reasons. One is to understand how nonspherical droplets assemble in systems whose rheology, texture, and quality are determined by the droplet microstructure. Second is to map the motion of

Received: June 28, 2018
Revised: September 20, 2018
Published: September 21, 2018

DOI: 10.1021/acs.langmuir.8b02136
Langmuir 2018, 34, 12379−12386

nonspherical shapes driven by the competing effects of interfacial liquid meniscus motion and droplet mechanical properties. Dynamic shape change using physical mechanisms, such as geometry and interfacial driving forces,[34] will be a critical aspect of future directed and active material assembly efforts at the nanoscale, where Brownian motion is significant,[35] and at the microscale, where thermal motion no longer dominates.[36,37]

We study here the binary arrested coalescence of monodisperse ellipsoidal droplets with controlled aspect ratios (ARs) produced in a millifluidic device. Because of the importance of motion to shape-change and of final state to self-assembly, we examine both aspects here. We first explore the dynamics of an ellipsoidal droplet being pulled around another by a fluid meniscus as a means of understanding possible shape-change and self-assembly mechanisms. Many more configurations are possible for arrested pairs of ellipsoidal droplets than for spherical droplets, and we use the results of an energy minimization model to map the full extent of possible behavior while comparing to experimental findings.

EXPERIMENTAL SECTION

Methods and Materials. Oil-in-water emulsions were prepared by combination of an oil and aqueous phase during microchannel flow. The system has been characterized in a number of past works[11,19,26,27,38] and is an analogue of more complex systems such as milk fat.[39] The aqueous phase was a dispersion of neutralized 0.15% w/w Carbopol 846. The oil phase was a mixture of petrolatum containing 50% wax solids (Unilever) and varying levels of hexadecane (99% Sigma-Aldrich) to form mixtures containing either 30 or 40% w/w wax solids. The two components were heated to T = 80 °C until the petrolatum melted and fully mixed with hexadecane. The mixture then crystallized as a dispersion of solid crystals inside a liquid oil phase that can be emulsified.[11]

Millifluidics. Droplets were generated in a two-part co-flow millifluidic device made from a round 1.1 mm ID glass capillary (VitroCom), with a 90 μm ID tip created using a model P-97 micropipette puller (Sutter Instruments), inserted into a 1.1 mm ID square capillary (VitroCom). The oil phase was pumped through the inner, round capillary, whereas the continuous phase flows through the outer square tube.[40] Droplets with varying sizes and ARs were produced at a rate of roughly 6 to 10 per second by adjusting the dispersed phase flow rate between 0.08 and 1.2 mL/min while keeping the continuous phase at 0.08 mL/min. A movie of raw droplets being produced is included in the Supporting Information.

As seen in Figure 1A, droplets with irregular shapes were first produced as a result of the yield stress of the droplet phase (σ_y = 1−500 Pa).[26,27] Relatively uniform ellipsoidal shapes were then produced by immediately passing the dispersion through a section of the channel held at 40 °C by an external heating source.[41,42] The internal structure of the droplet partially melts during this step, reducing its yield stress and reshaping the droplet to a uniform ellipsoid with a maximum curvature set by the equality of the droplet and continuous phase yield stress values.[26−28] The yield stress of the 0.15% w/w aqueous Carbol 846 continuous phase (σ_y = 4.3 Pa) created a "liquid mold" environment that preserved the deformed droplet shape until it could cool and fully regain its own yield stress.[43,44] Image analysis of calibrated experimental micrographs was carried out using ImageJ software[45] to quantify droplet size, AR, center of mass, and long axis orientation. Error in the sizing and determination of center location arises from small variations from a perfect ellipse, as well as image resolution, contributing an average error of ∼2 μm. Doublets are studied only when they are level in the image plane to avoid errors from out-of-plane movements, consistent with our theoretical descriptions. We verify that no out-of-plane ellipsoid movement occurs by tracking the position of bright spots on droplet surfaces.

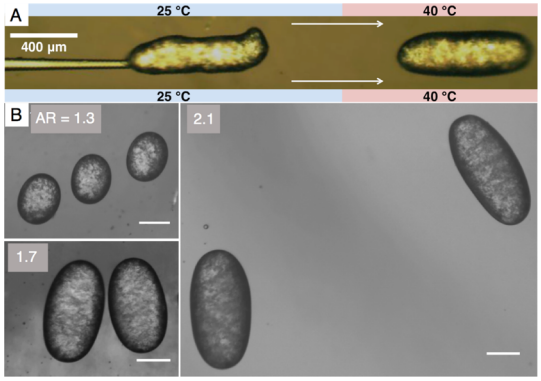

Figure 1. (A) Microscopic images within the millifluidic setup used to produce ellipsoidal droplets. An external yield stress fluid acts as a liquid mold to retain the high droplet AR during flow and heating. Melting and recrystallization after droplet production ensure that a uniform ellipsoidal shape is produced, even with nonuniform starting shapes like the one on the left. (B) Images of three different AR droplets produced by the millifluidic setup. The scale bar is 200 μm.

Figure 1B shows three examples of different AR ellipsoids produced using this method. On the basis of their maximum curvature, the three ellipsoid shapes in Figure 1B experience a maximum interfacial Laplace pressure range of 150−180 Pa for an interfacial tension of γ = 10 mN/m. The range is close to the maximum bulk yield stress previously measured for droplets with this solid concentration, $\sigma_y \approx$ 200 Pa.[26] The anisotropic shapes are stable despite being so close to their point of failure. The stability of the ellipsoids is likely enhanced by differences in the size of wax crystals formed in regions of the droplet with different curvatures. Prileszky and Furst[41] found enhanced droplet strength during microfluidic production of flattened spherocylinders from the same materials used here. They noted that regions of high curvature formed crystals with much smaller sizes than in other parts of the droplet, enhancing droplet stability because yield stress scales inversely with the crystal size in a dispersion.[41]

Coalescence studies were carried out by carefully transferring droplets to a volume of aqueous 0.3% w/w microfibrous cellulose yield stress (σ_y = 0.5 Pa) fluid[46] that prevents droplet drift but does not hinder coalescence and reorientation. Micromanipulation was performed on droplets, inside a small liquid sample placed on glass slides, using a three-axis system (Narishige International) mounted on an inverted microscope (Motic AE31). Droplets were grasped, using suction applied by adjusting the height of a small fluid reservoir connected to a microcapillary in the sample volume, and then the droplets were pushed together by slow manipulation to initiate coalescence by overcoming the liquid disjoining pressure.[10]

RESULTS AND DISCUSSION

Arrested coalescence can occur when the elasticity of an internal solid network in two droplets is sufficient to balance the interfacial Laplace pressure during some stage of the coalescence process.[11] As a result, the balance can be altered by, for example, increasing the internal solid concentration of the droplets in order to increase the droplet elasticity. When the symmetry of the system is broken, for example, when a third droplet is added to an existing arrested pair, reorientation can occur when the meniscus pulls the droplets in a direction that minimizes the assembly's surface energy.[19] We consider the potential for such effects on ellipsoidal droplets here by studying the simplistic case of an ellipse rolling around a second one.

Rolling Ellipse Model. If the experimental droplets behave as hard solids when moved around one another, a simple rolling ellipse model can be used to study some aspects of the

DOI: 10.1021/acs.langmuir.8b02136
Langmuir 2018, 34, 12379−12386

droplet motion. We focus here on ellipse motion, rather than ellipsoids, as the latter case is far more complex[47] and so ensure that the experimental motion of the ellipsoids proceeds in a single plane. The rolling ellipse model also provides a basis for comparison with experimental results using droplets that can undergo some degree of deformation as a result of their internal elastic network.[11] The two-dimensional path of the center of an ellipse rolling around another, congruent, ellipse is described in Cartesian coordinates by the curve[48]

$$(x^2 + y^2)^2 = 4a^2x^2 + 4b^2y^2 \quad (1)$$

where a and b are the major and minor axes of each ellipse and the AR is defined as

$$\mathrm{AR} \equiv \frac{a}{b} \quad (2)$$

Equation 1 assumes that motion of the ellipses begins with the two shapes aligned end-to-end along their long axes and ignores slip between the two shapes during motion. Visualizations of calculated ellipse paths were produced using the code developed by Mahieu.[49] Figure 2A shows several plots of

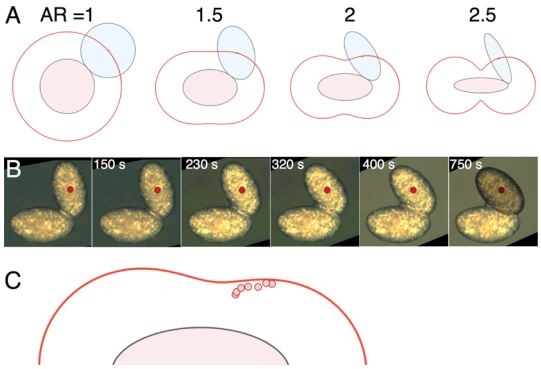

Figure 2. (A) Paths plotted in red for the center of mass of various ellipses rolling around a second one. Increasing the AR alters the path of the center of mass, varying the path curvature when the two shapes are aligned edge-to-edge. (B) Experimental micrographs of two ellipsoidal droplets containing 40% solids as they undergo arrested coalescence and reorientation. (C) Plotted positions of the center of mass of the upper ellipsoid in (B) as compared to the calculated path of a system with the same dimensions using eq 1.

the calculated trajectory, in red, of the center of mass of a blue ellipse, rolling around the perimeter of a second, identical, red ellipse. As the AR of the ellipses increases, the moving ellipse path transitions from perfectly circular, for AR = 1, to an increasingly complex path. Regions of the path with sharp changes in curvature are evident when the ellipses are aligned edge-to-edge, increasing in magnitude as the ellipse AR increases. Figure 2B shows a series of images of two ellipsoidal droplets just after coalescence has initiated. Here, the images have been rotated to fix the position of the lower droplet and enhance study of subsequent changes. The liquid film bridging the droplets radially moves out from the point of initial contact, reducing overall surface energy, and in the process pulls the two droplets together. Similar behavior was seen in the case of two spherical droplets undergoing arrested coalescence.[11] However, here, the nonspherical droplets also experience a change in relative orientation as the interfacial force pulling them together rolls one droplet along the edge of the other, similar to the action of ellipsoidal gears.[50] A red dot has been placed at the center of mass of the upper ellipsoid, allowing us to track changes in orientation as a result of the meniscus movement. The droplets largely move as rigid bodies and never move in a way that increases surface area, consistent with previous observations of spherical droplets moved by meniscus effects.[19] There is also some noticeable deformation of the droplets as the meniscus pulls them together in the last frame of Figure 2B, where overlap with the other ellipse is apparent, also in agreement with the behavior of spherical droplets.[11] We highlight this effect using a drawn ellipse overlay in Figure 2B that indicates the degree of overlap of the drops as a result of elastic deformation.[11] The last frame in Figure 2B represents the final stable position of this doublet, even though we might naively expect the two droplets to relax further and touch long edges. Some resistance to the reduction of surface energy must be acting to halt further motion, perhaps because of local friction or deformation of the internal elastic microstructure. Comparison of the center of mass positions in Figure 2B with calculated paths for this doublet will allow us to quantify the magnitude of any effects on the trajectory.

In Figure 2C, we plot a calculated trajectory following the method used to generate Figure 2A, along with the experimentally determined positions of the center of mass of the upper droplet in Figure 2B to assess any nonidealities. We see good general agreement of the experimental and calculated paths, though the real droplet is systematically closer to the second droplet than predicted. The deviation likely results from the small strain the droplets experience as the internal solid network deforms elastically.[11] The last few points in Figure 2C deviate more significantly from the calculated path, indicating that there may be stronger deformation occurring late in the process and that such deviations are time- and position-dependent. Variations in the deformation during arrested coalescence between the two droplets will cause variations in frictional resistance to movement, complicating our description of the process. We do not quantify strain in these systems, as we did for spherical droplets,[11] as the more complex ellipsoidal shape here complicates such a description. The two-dimensional calculations do not fully account for the three-dimensional nature of the ellipsoids produced here and also ignore the effects of the liquid film between droplets. They do, however, communicate the basic principle at work here: the movement of one ellipsoidal droplet around another's perimeter is a strong function of the varying curvature of the ellipsoids. Below, we improve on the above description, by simulating the three-dimensionality of the ellipsoids as well as the effects of the liquid film that imposes the stress driving motion, providing a more comprehensive understanding of the arrested coalescence behavior of ellipsoidal droplets.

Surface Minimization Model. We simulated the fluid−fluid interface with *Surface Evolver*[51] to map the energy landscape of the ellipsoidal doublets as a function of their relative orientation only because of interfacial tension. Example code is included in the Supporting Information. The droplets are modeled as volumes of space from which the fluid−fluid interface is excluded and, in effect, must be "shrink-wrapped". These are implemented in *Surface Evolver* as one-sided level set constraints, around which the area of the fluid−fluid interface is minimized at a fixed enclosed volume as a function of the relative position of the two droplets. In the absence of these constraints, the interface would form the usual completely spherical shape; however, with them in place, the fluid−fluid

DOI: 10.1021/acs.langmuir.8b02136
Langmuir 2018, 34, 12379−12386

interface will tend to follow the constraint surface except around the contact point where a meniscus is formed depending on the available fluid volume. In our model, we suppose that the interface has uniform surface tension, and hence, the area of the interface is proportional to surface energy and minimizing the area is equivalent to minimizing the surface energy. In the previous work, this strategy allowed us to correctly predict the critical angle below which the menisci of two spherical droplets overlapped with that of a third added droplet, causing reconfiguration of the triplet shape.[19]

The computational geometry is depicted in Figure 3: the coordinate system is oriented such that the y axis is along the

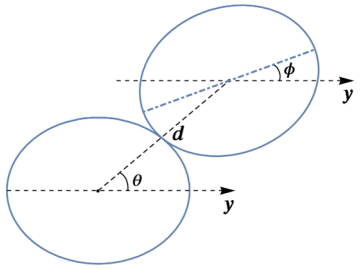

Figure 3. Coordinate system used to describe the relative position of two coalescing ellipsoidal droplets.

major axis of one of the ellipsoids. The center of mass of the other is at the zenithal angle θ from this axis and oriented at an angle ϕ to it. Because of the symmetry of the system, the domain of θ is from 0 to 90° and ϕ from 0 to 180°. For every θ and ϕ, the distance d is calculated using the overlap algorithm proposed by Perram and Wertheim[52] such that the second ellipsoid is positioned just in contact with the surface of the first ellipsoid. The ellipsoids each impose a level set constraint on the fluid interface

$$\mathbf{r}\Sigma^{-1}\mathbf{r} > 1 \tag{3}$$

$$(\mathbf{r} - \mathbf{r}_c)^T R^T \Sigma^{-1} R(\mathbf{r} - \mathbf{r}_c) > 1 \tag{4}$$

where $\mathbf{r} = (x, y, z)$, $\mathbf{r}_c$ is the center of the second ellipsoid at $(0, d\cos\theta, d\sin\theta)$, R is the rotational matrix of ϕ around the x axis, and Σ is the diagonal matrix with entries (b^2, a^2, b^2). Here, superscripts T and -1 refer to the standard linear algebra manipulations, transpose and inverse, respectively. One can interpret these constraints as follows: the surface of the first ellipsoid corresponds to a contour—that is, a level set—of the scalar function $\mathbf{r}\Sigma^{-1}\mathbf{r}$, specifically the contour where this function is equal to 1. This inequality constraint therefore requires that the fluid interface be strictly outside the first ellipsoid. The second constraint is similar, but incorporates rotation and translation to shift the contour to correspond to the first ellipsoid.

The surface is also minimized with a fixed volume $V = 2 \times \frac{4\pi}{3}ab^2/0.95$, slightly greater than the volume of the two ellipsoids in order to allow the formation of a meniscus. This mimics the experimental system, where deformation of the internal matrix upon initial contact of the droplets is accompanied by release of a fluid fraction that forms the meniscus. We assume that the amount of available fluid is constant as a function of orientation. This is a rough approximation, as one should properly simultaneously minimize the energy with respect to elastic deformation of the solid fraction as well as the fluid interface. We eschew this approach presently as we focus only on the role of interfacial tension.

The surface to be minimized is discretized within *Surface Evolver* as a polyhedral triangular mesh, and the area of this mesh is minimized, subject to constraints, with respect to the total area of the polyhedron by the conjugate gradient method. During the minimization, a number of mesh quality control measures are performed, such as breaking up triangles that are large or in regions of large curvature. Full implementation details are available,[51] and a sample script for our problem is included as the Supporting Information.

Results from the simulation are displayed in Figure 4, which shows a contour plot of the surface energy, for ellipsoids of AR = 1.2, calculated using *Surface Evolver* simulations for the entire range of angles θ and ϕ. Three-dimensional renderings of simulated ellipsoidal droplet pairs are also shown for representative regions to aid the interpretation of the results and allow comparison with the experiment. Two minimum surface energy regions are visible at high θ values in combination with either low or high ϕ values, consistent with the case when two ellipsoids are joined at their long edges and minimize their total surface area. A maximum in surface energy occurs where the two ellipsoidal droplets are parallel and arranged end on, at low θ values in combination with either low or high ϕ values, maximizing the doublet surface area. A saddle point exists where the droplets are

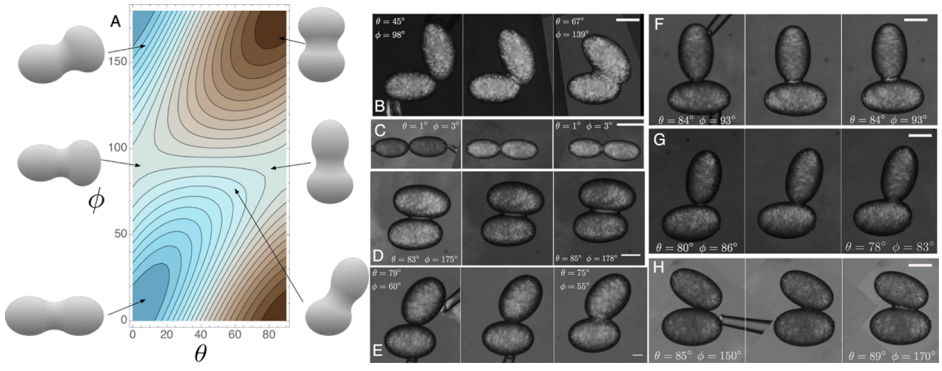

Figure 4. (A) Density plot of surface energy as a function of θ and ϕ for ellipsoid AR = 1.2. High-energy regions are colored cyan, whereas low-energy regions are brown, with neutral colors indicating intermediate saddle regions. Six three-dimensional renderings of exemplary configurations are shown for representative energy extrema. (B–H) Stable experimental examples of some of the simulated shapes are shown for droplets with a solid content of 40% and AR = 1.6.

DOI: 10.1021/acs.langmuir.8b02136
Langmuir 2018, 34, 12379–12386

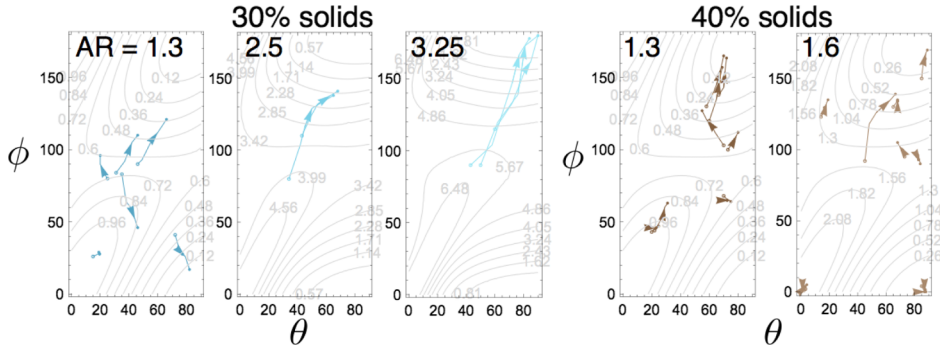

Figure 5. Experimental pathways of ellipsoidal doublets relaxing to their final configuration are plotted on several calculated surface energy contour maps for different ARs. Arrows indicate direction of movement on each trajectory. Increasing the AR changes the shape of the extrema regions, as a result of the changes in ellipsoid geometry, and also enables relaxation to lower energy states for 30% solids.

perpendicularly aligned in a "T" configuration. An analogous energy diagram was computed for single nanocylinders at a flat liquid interface, finding similar regions of stability for similar orientations.[53]

Generally, when the droplets initially make contact at arbitrary angles, we expect their orientation to evolve down the energy gradient toward the minimum because the motion occurs in a viscous quasistatic regime, a prediction that will be robustly tested in the subsequent section. The droplets in the doublet are, however, also subject to forces from the internal structure and the opposing meniscus driving forces on the ellipsoid surface. Divergence from the behavior predicted by surface energy alone therefore allows us to assess the relative importance of these other terms to the final shape of the doublet.

Figure 4B−H shows several examples of experimental ellipsoidal doublets forming and reorienting, to various degrees, before reaching their final arrested state. The droplets all have an aspect ratio of AR ≈ 1.6 and contain 40% solids by weight. As a result, the droplet deformation is expected to be relatively low during arrested coalescence and any observed reorientation by the fluid meniscus will be reproducible and easily compared with the predictions of Figure 4A. Figure 4A suggests that we might only find stable configurations of ellipsoidal doublets at the two energy minima. However, Figure 4B−H shows that a much wider range of final doublet states can be formed, without necessarily exhibiting the reorientation we might expect. Figure 4B,H shows the largest amount of reorientation, with ϕ varying by 40° and 20°, respectively. In Figure 4B, the reorientation halts with the two ellipsoids oriented at angles of θ = 67° and ϕ = 139°, close to the energy minimum in Figure 4A but several contour lines outside of it. Clearly, some type of constraint force, possibly the elastic resistance of the internal structure, affects the reorientation process and can arrest the system at a point that is not stationary with respect to the surface tension term. In Figure 4H, an energetic minimum is attained by the pair of ellipsoids at values of θ = 89° and ϕ = 170°. Other initial states lead to much less reorientation, expanding the range of forms that can be obtained by ellipsoidal droplet arrested coalescence. Because the ellipsoidal droplet shape is anisotropic, this implies that the initial orientation of the droplets' major axes will have a strong effect on the subsequent reorientation brought about by the meniscus.

Figure 4C−G reorients very little from their initial position, moving at most 5° in Figure 4E. In Figure 4C, two ellipsoids initiate contact at angles of θ = 1° and ϕ = 3° and do not experience any reorientation over time, despite this representing the highest energy configuration calculated in Figure 4A. This is because the meniscus forces that normally drive reorientation vanish at an energetic maximum, creating an unstable stationary state. However, additional influences present, such as elastic resistance of the internal structure, may stabilize the stationary state against collapse. Figure 4D shows the case when two ellipsoids are initially brought together into the minimum energy configuration at the top right of Figure 4A. Here, the system reorients only very slightly. Figure 4E−G also does not reorient significantly, and they all come into contact in various realizations of the saddle point conditions in Figure 4A, an area of intermediate stability where two ellipsoids are arrested at, or near, right angles to one another. The system may be stabilized at the saddle point, as in Figure 4F. If the doublet is initially configured slightly away from the saddle point, as in Figure 4E,G, the system evolves toward the energy minimum slightly but nonetheless is arrested close to the saddle point. Again, this may be explained by the additional constraint forces from the internal structure.

Because the ellipsoid dimensions determine the amount and distribution of surface area in the droplets, we also explore the effects of droplet AR on our above results. Calculated energy contour plots are shown in Figure 5 for several ellipsoidal droplet ARs, as well as two different internal droplet solid levels. Our simulation can account for changes in solid level by varying the volume of fluid enclosed by the simulated interface, but we use a fixed value here because it does not change the shape of the energy contour plot. The contours in each plot are labeled with the surface energy relative to the surface energy minimum. Increasing AR alters the shape of the regions of energy minima and maxima as a result of the geometric changes in the droplets. For example, the width of the minimum energy region for the three ARs with 30% solids in Figure 5 increases as the AR increases, spanning a wider range of θ values. The effect is geometric and is caused by the higher ellipsoid edge length at larger AR values.

The instantaneous values of θ and ϕ for a number of experimental doublets, during coalescence and reorientation, are plotted as colored trajectory lines on top of the contour plots in Figure 5 to show the extent of reorientation that occurs for different starting positions and compositions. The contour plot provides a useful map to summarize many different experiments and compare the effects of multiple system variables. For droplets containing 30% solids, at all ARs, the trajectories plotted in Figure 5 all move in the direction of decreasing energy. Interestingly, for AR = 1.3, most do not

DOI: 10.1021/acs.langmuir.8b02136
Langmuir 2018, 34, 12379−12386

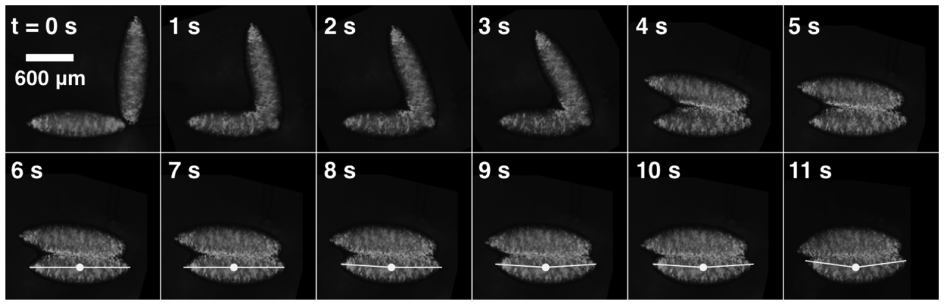

Figure 6. Arrested coalescence of high AR ellipsoidal droplets, AR = 3.7, containing 30% solids. The doublet exhibits deformation of the ellipsoid being moved, curving it around the second droplet.

reach a minimum, consistent with the example in Figure 4B, likely because of inherent solid and fluid resistance to flow and movement. As the AR of the droplets containing 30% solids is increased in Figure 5, the lengths of the trajectories increase significantly, indicating a greater degree of movement and reorientation during arrested coalescence. Although fewer data were taken for the larger ARs, droplets with AR = 2.5 and AR = 3.25 reproducibly move from an intermediate stability level, at a calculated saddle point, entirely into the minimum energy region. Despite the simplicity of the model, agreement between experimental and predicted final configurations is surprisingly good when meniscus-induced reorientation is this significant. It is reasonable to expect that longer ellipsoids will have stronger driving forces to reduce surface energy, reorienting much more significantly than droplets with smaller ARs. The concept of a driving force, here reduction of surface energy, and a resistance, here an elastic or frictional force, suggests that increasing droplet solid level and elasticity will also affect the reorientation process.

Figure 5 plots trajectories for a number of doublet systems containing 40% solids as they reorient. For an AR = 1.3, the trajectory sizes are of similar or smaller size compared to the trajectories of the droplets containing 30% solids in Figure 5. At the higher solid level in Figure 5, most of the reorientation observed at both ARs moves the doublets down the energy gradient but does not move them into the calculated energy minimum state, likely because of a larger elastic resistance to deformation. Interestingly, we observe two instances at 40% solids where the droplets move up the energy gradient, possibly because of heterogeneities in the solid structure of the droplet. Even more extreme effects of the larger ARs are observed at the lower solid concentration studied.

The top row of Figure 6 shows a time sequence of images of two ellipsoids containing 30% solids, with AR = 3.7, as they are brought together, begin coalescence, and then arrest. The ellipsoids in Figure 6 have a high maximum curvature as a result of their high AR. The droplets experience a maximum interfacial Laplace pressure of ∼400 Pa for an interfacial tension of γ = 10 mN/m, but at 30% solids, their maximum yield stress is only $\sigma_y \approx 1$ Pa.[26] As noted earlier, these anisotropic droplets likely possess enhanced stability because of crystallization of small crystals in their high curvature regions,[41] but we are unable to study this effect in detail here.

The images in Figure 6 are captured between crossed polarizers to highlight the solid-phase regions of the structures as they move. Because the crystals are anisotropic, we should see an increase in birefringence where flow occurs and aligns the crystals. We do see some evidence of this in Figure 6, for example, at 3−5 s, as the oil meniscus expands and crystals on the edge of both droplets are aligned.

In the first few frames of Figure 6, the droplets move together steadily because of migration of the fluid meniscus, reducing doublet surface area, and moving it from a relatively high-energy configuration, near the saddle point in the middle of Figure 4A, toward the low-energy region of the upper-right quadrant of Figure 4A. The time interval is the same for each frame, but the distance moved from the frame at t = 3 s to the frame at 4 s is about 300 μm, a significant acceleration. Much like elliptical gears, we find that ellipsoidal droplets can convert a relatively constant driving force, expansion of the fluid meniscus, into a variable speed movement. Such forces also have a strong effect on the individual droplets.

The bottom row of Figure 6 highlights the behavior of the two droplets after reaching a near-final conformation: edge-to-edge alignment in a low-energy state. An overlaid line, connecting the lower ellipsoid's endpoints with its midpoint, is used to visualize the subsequent deformation of the ellipsoid as the meniscus continues to expand completely across the length of the doublet. Here, the deflection of the lower ellipsoid is ∼120 μm in the last frame, about 10% of the ellipsoid length. The significant deformation of the ellipsoids by the meniscus force only occurs once the droplets have been brought together at the energetic minimum with respect to their relative orientation. At this point, no further reduction in the meniscus area can occur by rotations; however, deformation of the ellipsoids can bring their ends into closer contact, reducing the overall contact area at the expense of elastic reorganization of the internal structure. Such deformation is only observed when droplets have low solid levels and high ARs, so the higher solid level droplets avoid deformation because of their increased elastic resistance to droplet deformation.[26−28]

■ CONCLUSIONS

The processes of self-assembly and reorientation of pairs of ellipsoidal droplets undergoing arrested coalescence have been studied here using stable poroelastic droplets, produced in a millifluidic process, with varying ARs. The ellipsoidal shape of the droplets enables reorientation and deformation behavior that is significantly different from that exhibited by spherical droplets.[19] Ellipsoidal droplets experience more complex trajectories and a wider range of motion, than spheres[19] during meniscus-driven reorientation. The experimentally observed dynamics approach but do not always attain theoretical predictions of the most stable configurations with respect to geometry and surface energy. Small amounts of deformation occur for all droplets, reducing the radius of their

DOI: 10.1021/acs.langmuir.8b02136
Langmuir 2018, 34, 12379−12386

path when compared to that predicted by the locus of an ellipse rotating around a second ellipse. The final configuration of the droplets also deviates from more developed three-dimensional simulations of arrested coalescence of ellipsoids, likely because of elastic and frictional resistance to the stresses transmitted by the fluid meniscus. The resistance can be tuned by adjusting the dimensions and solid fraction of the droplets, potentially allowing control of larger structure assembly and reorientation.

We are particularly interested in how irregularly shaped, non-Brownian droplets can be assembled by a fluid meniscus to achieve changes in shape and to form larger-scale structures. This work demonstrates limits on the ability to control shape-change and other dynamics using viscoelastic droplets. Varying the AR of the droplets controls the extent of reorientation that is possible before a stable configuration is reached. All ellipsoidal droplets experience some reorientation, mostly moving toward lower surface energy states. Low AR ellipsoids form mostly metastable configurations during reorientation, whereas higher ARs mostly converge to energy minima, though increased elasticity can offset such effects. Tuning the rheology of the droplets impacts the final configurations, likely by affecting the significance of local and variable deformation of individual droplets. The importance of this work is its droplet-level study of arrested coalescence and reorientation mechanisms for nonspherical shapes. It is hoped that the insights can be used to create accurate predictions of larger-scale aggregates formed via assembly and meniscus-driven dynamics,[24] enabling design of emulsion microstructures and their mechanical properties.[28] Applications are possible in areas as diverse as food product development,[25] advanced material creation,[54] and additive manufacturing.[24]

■ ASSOCIATED CONTENT

Supporting Information

The Supporting Information is available free of charge on the ACS Publications website at DOI: 10.1021/acs.langmuir.8b02136.

Movie of microscopic production of several irregular droplets by millifluidic flow of a hexadecane−petrolatum mixture into an aqueous Carbopol solution (ZIP)

Example file of *Surface Evolver* code used to perform the energetic simulations of ellipsoid pairs (ZIP)

■ AUTHOR INFORMATION

Corresponding Author

*E-mail: p.spicer@unsw.edu.au.

ORCID

Patrick T. Spicer: 0000-0002-8562-3906

Notes

The authors declare no competing financial interest.

■ ACKNOWLEDGMENTS

This material is based upon work supported by the National Science Foundation under grant no. DMR-1654283.

■ REFERENCES

(1) *Food emulsions*; Friberg, S., Larsson, K., Sjoblom, J., Eds.; CRC Press, 2004; Vol. *132*.

(2) Gupta, A.; Eral, H. B.; Hatton, T. A.; Doyle, P. S. Nanoemulsions: formation, properties and applications. *Soft Matter* **2016**, *12*, 2826−2841.

(3) Vandebril, S.; Vermant, J.; Moldenaers, P. Efficiently suppressing coalescence in polymer blends using nanoparticles: role of interfacial rheology. *Soft Matter* **2010**, *6*, 3353.

(4) Zylyftari, G.; Ahuja, A.; Morris, J. F. Modeling oilfield emulsions: comparison of cyclopentane hydrate and ice. *Energy Fuels* **2015**, *29*, 6286−6295.

(5) Claessens, M. M. A. E.; Tharmann, R.; Kroy, K.; Bausch, A. R. Microstructure and viscoelasticity of confined semiflexible polymer networks. *Nat. Phys.* **2006**, *2*, 186−189.

(6) Pontani, L.-L.; Jorjadze, I.; Viasnoff, V.; Brujic, J. Biomimetic emulsions reveal the effect of mechanical forces on cell-cell adhesion. *Proc. Natl. Acad. Sci. U.S.A.* **2012**, *109*, 9839−9844.

(7) Mohraz, A. Interfacial routes to colloidal gelation. *Curr. Opin. Colloid Interface Sci.* **2016**, *25*, 89−97.

(8) Bdzil, J. B.; Stewart, D. S. The Dynamics of Detonation in Explosive Systems. *Annu. Rev. Fluid Mech.* **2007**, *39*, 263−292.

(9) Studart, A. R.; Shum, H. C.; Weitz, D. A. Arrested Coalescence of Particle-coated Droplets into Nonspherical Supracolloidal Structures†. *J. Phys. Chem. B* **2009**, *113*, 3914−3919.

(10) Pawar, A. B.; Caggioni, M.; Ergun, R.; Hartel, R. W.; Spicer, P. T. Arrested coalescence in Pickering emulsions. *Soft Matter* **2011**, *7*, 7710−7716.

(11) Pawar, A. B.; Caggioni, M.; Hartel, R. W.; Spicer, P. T. Arrested coalescence of viscoelastic droplets with internal microstructure. *Faraday Discuss.* **2012**, *158*, 341−350.

(12) Boode, K.; Walstra, P. Partial coalescence in oil-in-water emulsions 1. Nature of the aggregation. *Colloids Surf., A* **1993**, *81*, 121−137.

(13) Fredrick, E.; Walstra, P.; Dewettinck, K. Factors governing partial coalescence in oil-in-water emulsions. *Adv. Colloid Interface Sci.* **2010**, *153*, 30−42.

(14) van der Kooij, H. M.; Sprakel, J. Watching paint dry; more exciting than it seems. *Soft Matter* **2015**, *11*, 6353−6359.

(15) Manoharan, V. N.; Elsesser, M. T.; Pine, D. J. Dense Packing and Symmetry in Small Clusters of Microspheres. *Science* **2003**, *301*, 483−487.

(16) Sacanna, S.; Irvine, W. T. M.; Chaikin, P. M.; Pine, D. J. Lock and key colloids. *Nature* **2010**, *464*, 575−578.

(17) Sacanna, S.; Pine, D. J. Shape-anisotropic colloids: Building blocks for complex assemblies. *Curr. Opin. Colloid Interface Sci.* **2011**, *16*, 96−105.

(18) Nabavi, S. A.; Vladisavljević, G. T.; Zhu, Y.; Manović, V. Synthesis of Size-Tunable CO2-Philic Imprinted Polymeric Particles (MIPs) for Low-Pressure CO2 Capture Using Oil-in-Oil Suspension Polymerization. *Environ. Sci. Technol.* **2017**, *51*, 11476−11483.

(19) Dahiya, P.; DeBenedictis, A.; Atherton, T. J.; Caggioni, M.; Prescott, S. W.; Hartel, R. W.; Spicer, P. T. Arrested coalescence of viscoelastic droplets: triplet shape and restructuring. *Soft Matter* **2017**, *13*, 2686−2697.

(20) Basavaraj, M. G.; Fuller, G. G.; Fransaer, J.; Vermant, J. Packing, Flipping, and Buckling Transitions in Compressed Monolayers of Ellipsoidal Latex Particles. *Langmuir* **2006**, *22*, 6605−6612.

(21) Madivala, B.; Fransaer, J.; Vermant, J. Self-Assembly and Rheology of Ellipsoidal Particles at Interfaces. *Langmuir* **2009**, *25*, 2718−2728.

(22) Yunker, P. J.; Still, T.; Lohr, M. A.; Yodh, A. G. Suppression of the coffee-ring effect by shape-dependent capillary interactions. *Nature* **2011**, *476*, 308−311.

(23) Phillips, C. L.; Jankowski, E.; Krishnatreya, B. J.; Edmond, K. V.; Sacanna, S.; Grier, D. G.; Pine, D. J.; Glotzer, S. C. Digital colloids: reconfigurable clusters as high information density elements. *Soft Matter* **2014**, *10*, 7468−7479.

(24) Prileszky, T. A.; Furst, E. M. Fluid networks assembled from endoskeletal droplets. *Chem. Mater.* **2016**, *28*, 3734−3740.

(25) Kim, J.; Vanapalli, S. A. Microfluidic Production of Spherical and Nonspherical Fat Particles by Thermal Quenching of Crystallizable Oils. *Langmuir* **2013**, *29*, 12307−12316.

DOI: 10.1021/acs.langmuir.8b02136
Langmuir 2018, 34, 12379−12386

(26) Caggioni, M.; Bayles, A. V.; Lenis, J.; Furst, E. M.; Spicer, P. T. Interfacial stability and shape change of anisotropic endoskeleton droplets. *Soft Matter* **2014**, *10*, 7647−7652.
(27) Caggioni, M.; Lenis, J.; Bayles, A. V.; Furst, E. M.; Spicer, P. T. Temperature-Induced Collapse, and Arrested Collapse, of Anisotropic Endoskeleton Droplets. *Langmuir* **2015**, *31*, 8558−8565.
(28) Bayles, A. V.; Prileszky, T. A.; Spicer, P. T.; Furst, E. M. Model of Structured Emulsion Droplet Stability and Reconfigurability. *Langmuir* **2018**, *34*, 4116−4121.
(29) Spicer, P.; Caggioni, M.; Lenis, J.; Bayles, A. Shape-Changing Droplet. European Patent EP 2909299 B1; Procter and Gamble Co., 2017.
(30) Spicer, P.; Caggioni, M.; Lenis, J.; Bayles, A. Non-Spherical Droplet. U.S. Patent 9,597,648 B2; Procter and Gamble Co., 2017.
(31) Giermanska, J.; Thivilliers, F.; Backov, R.; Schmitt, V.; Drelon, N.; Leal-Calderon, F. Gelling of Oil-in-Water Emulsions Comprising Crystallized Droplets. *Langmuir* **2007**, *23*, 4792−4799.
(32) Thivilliers, F.; Laurichesse, E.; Saadaoui, H.; Leal-Calderon, F.; Schmitt, V. Thermally Induced Gelling of Oil-in-Water Emulsions Comprising Partially Crystallized Droplets: The Impact of Interfacial Crystals. *Langmuir* **2008**, *24*, 13364−13375.
(33) Thivilliers-Arvis, F.; Laurichesse, E.; Schmitt, V.; Leal-Calderon, F. Shear-Induced Instabilities in Oil-in-Water Emulsions Comprising Partially Crystallized Droplets. *Langmuir* **2010**, *26*, 16782−16790.
(34) Péraud, J.-P.; Lauga, E. Geometry and wetting of capillary folding. *Phys. Rev. E: Stat., Nonlinear, Soft Matter Phys.* **2014**, *89*, 043011.
(35) Cho, J.-H.; James, T.; Gracias, D. H. Curving nanostructures using extrinsic stress. *Adv. Mater.* **2010**, *22*, 2320−2324.
(36) Py, C.; Reverdy, P.; Doppler, L.; Bico, J.; Roman, B.; Baroud, C. N. Capillary origami: spontaneous wrapping of a droplet with an elastic sheet. *Phys. Rev. Lett.* **2007**, *98*, 156103.
(37) Leong, T. G.; Lester, P. A.; Koh, T. L.; Call, E. K.; Gracias, D. H. Surface tension-driven self-folding polyhedra. *Langmuir* **2007**, *23*, 8747−8751.
(38) Dahiya, P.; Caggioni, M.; Spicer, P. T. Arrested coalescence of viscoelastic droplets: polydisperse doublets. *Philos. Trans. R. Soc., A* **2016**, *374*, 20150132.
(39) Thiel, A. E.; Hartel, R. W.; Spicer, P. T.; Hendrickson, K. J. Coalescence Behavior of Pure and Natural Fat Droplets Characterized via Micromanipulation. *J. Am. Oil Chem. Soc.* **2016**, *93*, 1467−1477.
(40) Utada, A. S.; Lorenceau, E.; Link, D. R.; Kaplan, P. D.; Stone, H. A.; Weitz, D. A. Monodisperse double emulsions generated from a microcapillary device. *Science* **2005**, *308*, 537−541.
(41) Prileszky, T. A.; Furst, E. M. Crystallization Kinetics of Partially Crystalline Emulsion Droplets in a Microfluidic Device. *Langmuir* **2016**, *32*, 5141−5146.
(42) Caggioni, M.; Traini, D.; Young, P. M.; Spicer, P. T. Microfluidic production of endoskeleton droplets with controlled size and shape. *Powder Technol.* **2018**, *329*, 129−136.
(43) Pairam, E.; Vallamkondu, J.; Koning, V.; van Zuiden, B. C.; Ellis, P. W.; Bates, M. A.; Vitelli, V.; Fernandez-Nieves, A. Stable nematic droplets with handles. *Proc. Natl. Acad. Sci. U.S.A.* **2013**, *110*, 9295−9300.
(44) Burke, C. J.; Mbanga, B. L.; Wei, Z.; Spicer, P. T.; Atherton, T. J. The role of curvature anisotropy in the ordering of spheres on an ellipsoid. *Soft Matter* **2015**, *11*, 5872−5882.
(45) Schneider, C. A.; Rasband, W. S.; Eliceiri, K. W. NIH Image to ImageJ: 25 years of image analysis. *Nat. Methods* **2012**, *9*, 671−675.
(46) Emady, H.; Caggioni, M.; Spicer, P. Colloidal microstructure effects on particle sedimentation in yield stress fluids. *J. Rheol.* **2013**, *57*, 1761−1772.
(47) Krakowski, K. A.; Leite, F. S. Geometry of the rolling ellipsoid. *Kybernetika* **2016**, *52*, 209−223.
(48) Abbena, E.; Salamon, S.; Gray, A. *Modern Differential Geometry of Curves and Surfaces with Mathematica*; Chapman and Hall/CRC, 2017.
(49) Mahieu, E. *Ellipse Rolling around Another Ellipse Project*; Wolfram Demonstrations, Published: July 15, 2014.
(50) Zarębski, I.; Sałaciński, T. Designing of non-circular gears. *Arch. Mech. Eng.* **2008**, *55*, 275−292.
(51) Brakke, K. A. The surface evolver. *Exp. Math.* **1992**, *1*, 141−165.
(52) Perram, J. W.; Wertheim, M. S. Statistical mechanics of hard ellipsoids. I. Overlap algorithm and the contact function. *J. Comput. Phys.* **1985**, *58*, 409−416.
(53) Lewandowski, E. P.; Searson, P. C.; Stebe, K. J. Orientation of a Nanocylinder at a Fluid Interface. *J. Phys. Chem. B* **2006**, *110*, 4283−4290.
(54) Feng, L.; Pontani, L.-L.; Dreyfus, R.; Chaikin, P.; Brujic, J. Specificity, flexibility and valence of DNA bonds guide emulsion architecture. *Soft Matter* **2013**, *9*, 9816−9823.

DOI: 10.1021/acs.langmuir.8b02136
Langmuir 2018, 34, 12379−12386